Synthesis and Group Electronegativity Implications on the Electrochemical and Spectroscopic Properties of Diferrocenyl *meso*-Substituted Porphyrins

Aurélien Auger and Jannie C. Swarts*

Department of Chemistry, University of the Free State, P.O. Box 339, Bloemfontein, 9300, Republic of South Africa

Received May 1, 2006

Two different condensations of appropriate dipyrromethanes and aldehydes resulted in two structural isomers of metal-free, *meso*-substituted diferrocenyldipentafluorophenyl porphyrins, one with the ferrocenyl groups in the 5,15 positions, **6**, and the other with the ferrocenyl groups in the 5,10 positions, **7**. UV/vis spectroscopic and cyclic voltammetric (CV) techniques could not unambiguously distinguish between the isomers, but ^{1}H NMR clearly distinguished between them. Use of the CH_2Cl_2/0.1M $[N(^nBu)_4][B(C_6F_5)_4]$ solvent/supporting electrolyte system allowed good resolution between the two ferrocenyl CV waves with $\Delta E^{\circ\prime} = 111$ and 115 mV for **6** and **7**, 102 mV for the Zn derivative of **6**, namely **8**, and 109 mV for **6**'s Ni derivative, **9**. $\Delta E^{\circ\prime}$ values for the Zn (**10**) and Ni (**11**) derivatives of **7** were 103 and 95 mV, respectively. The formal reduction potentials, $E^{\circ\prime}$, at which the two observed ring-based electrochemical reductions and one oxidation process were detected, varied in a manner that depended on the cationic electronegativities, χ_{Zn2+} or χ_{Ni2+}, of the coordinated central cations. Differences in $E^{\circ\prime}$ of **6**−**11** with respect to that of *meso* tetraphenyl porphyrin, 2Htpp, were found to be related to the group electronegativities, χ_{C6H5}, χ_{C6F5}, χ_{Fc}, and χ_{Fc+}, of each *meso* substituent.

Introduction

Porphyrins and their derivatives are well-known tetrameric macrocycles that, owing to their expanded aromatic π-electron system, display unique physical and chemical properties.[1] Their electrochemical[2] and spectrophysical[3] properties in particular make these macrocyclic chromophores and their derivatives ideal candidates to mimic biological processes found in nature.[4] Porphyrin derivatives show rich electrochemical behavior in that six[2] ring-centered redox processes may be observed, the metals coordinated in the macrocyclic cavity may be redox active,[5] and electroactive *meso* or β-pyrrole substituents[6] may further expand the broad variety of electrochemical processes that this class of compounds may exibit. The electrochemistry of a compound can often be strongly related to its activity as a prospective drug.[7] In addition, the aromatic porphyrin and related phthalocyanine macrocycles are well-known photosensitisers for use in photodynamic therapy.[8] In terms of fluorinated macrocycles, van Lier and co-workers found that a series of asymmetrically substituted fluorinated phthalocyanines are effective photosensitizers for the production of singlet oxygen.[9] The photochemical and electron transport activity of fluorinated porphyrins have also been investigated.[10]

Ferrocene-based materials, on the other hand, have found increasing use in transition metal catalyzed processes.[11] The powerful electron-donating properties of the ferrocenyl group (group electronegativity = 1.87)[12] cause ferrocene-based derivatives to represent an important class of ligands for use in coordination chemistry.[13] The biological activity of ferrocene derivatives in the treatment of cancer has also been the focus of many literature reports.[14]

Porphyrins with strong electron donor and acceptor groups have found applications as second-order nonlinear optical systems.[15] This generates the promise that asymmetrically

* To whom correspondence should be addressed. E-mail: swartsjc@mail.uovs.ac.za.

(1) (a) Walker, F. A. In *The Porphyrin Handbook*; Kadish, K. M., Smith, K. M., Guilard, R., Eds.; Academic Press: New York, 2000; Vol. 5, p 81 (b) Pandey, R. K.; Zheng, G. In *The Porphyrin Handbook*; Kadish, K. M., Smith, K. M., Guilard, R., Eds.; Academic Press: New York, 2000; Vol. 6, p 157.

(2) Kadish, K. M.; Royal, G.; Van Caemelbecke, E.; Gueletti, L. In *The Porphyrin Handbook*; Kadish, K. M., Smith, K. M., Guilard, R., Eds.; Academic Press: New York, 2000; Vol. 9, p 1.

(3) Ali, H.; van Lier, J. E. *Chem. Rev.* **1999**, *99*, 2379.

(4) Kadish, K. M.; Guo, N.; Van Caemelbecke, E.; Froiio, A.; Paolesse, R.; Monti, D.; Tagliatesta, P.; Boschi, T.; Prodi, L.; Boletta, F.; Zaccheroni, N. *Inorg. Chem.* **1998**, *37*, 2358.

(5) (a) Walker, F. A.; Beroiz, D.; Kadish, K. M. *J. Am. Chem. Soc.* **1976**, *98*, 3484. (b) Kadish, K. M.; Lin, X. Q.; Han, B. C. *Inorg. Chem.* **1987**, *26*, 1987.

(6) Beer, P. D.; Drew, M. G. B.; Jagessar, R. *J. Chem. Soc., Dalton Trans.* **1997**, 881.

(7) Swarts, J. C.; Swarts, D. M.; Maree, D. M.; Neuse, E. W.; La Madeleine, C.; Van Lier, J. E. *Anticancer Res.* **2001,** *21,* 2033.

(8) (a) Detty, M. R.; Gibson, S. L.; Wagner, S. J. *J. Med. Chem.* **2004**, *47*, 3897. (b) Ackroyd, R.; Kelty, C.; Brown, N.; Reed, M. *Photochem. Photobiol.* **2001**, *74*, 656.

(9) Sharman, W. M.; Van Lier, J. E. *Bioconjugate Chem.* **2005**, *16*, 1166.

(10) Nango, M.; Iida, K.; Kawakita, T.; Matsura, M.; Harada, Y.; Yamashita, K.; Tsuda, K.; Kimura, Y. *J. Chem. Soc., Chem. Commun.* **1992,** 545.

(11) (a) Hayashie, T. In *Ferrocenes: Homogeneous Catalysis, Organic Synthesis, Material Science*; Togni, A., Hayashi, T., Eds.; VCH: Weinheim, 1995; p 105. (b) Bishop, J. J.; Davison, A.; Katcher, M. L.; Lichtenberg, D. W.; Merril, R. E.; Smart, J. C. *J. Organomet. Chem.* **1971**, *22*, 241. (c) Cullen, W. R.; Woolins, J. D. *Coord. Chem. Rev.* **1981**, *39*, 1. (d) Marqading, D.; Klusacek, A.; Gokel, G.; Hoffman, P.; Ugi, I. *J. Am. Chem. Soc.* **1970**, *92*, 5389.

(12) Du Plessis, W. C.; Vosloo, T. G.; Swarts, J. C. *J.Chem. Soc., Dalton Trans.* **1998**, 2507.

(13) Togni, A. *Angew. Chem., Int. Ed.* **1996**, *108*, 1581.

(14) (a) Swarts, J. C. In *Macromolecular Symposia*; Guiseppi-Elie, A., Levon, K., Eds.; Wiley-VCH: Weinheim, 2002; Vol. 186, p 123. (b) Swarts, J. C.; Van Rensburg C. E. J. European patent 1345951, 2004.

(15) (a) Samyn, C.; Verbiest, T.; Persoons, A. *Macromol. Rapid Commun.* **2001**, *21*, 1. (b) Di Bella, S. *Chem. Soc. Rev.* **2001**, *30*, 355. (c) Kelley, A. M.; Leng, W.; Blanchard-Desce, M. *J. Am. Chem. Soc.* **2003**, *125*, 10520.

10.1021/om060373u CCC: $37.00
Publication on Web 12/07/2006

Scheme 1. Syntheses of Porphyrins 6−11

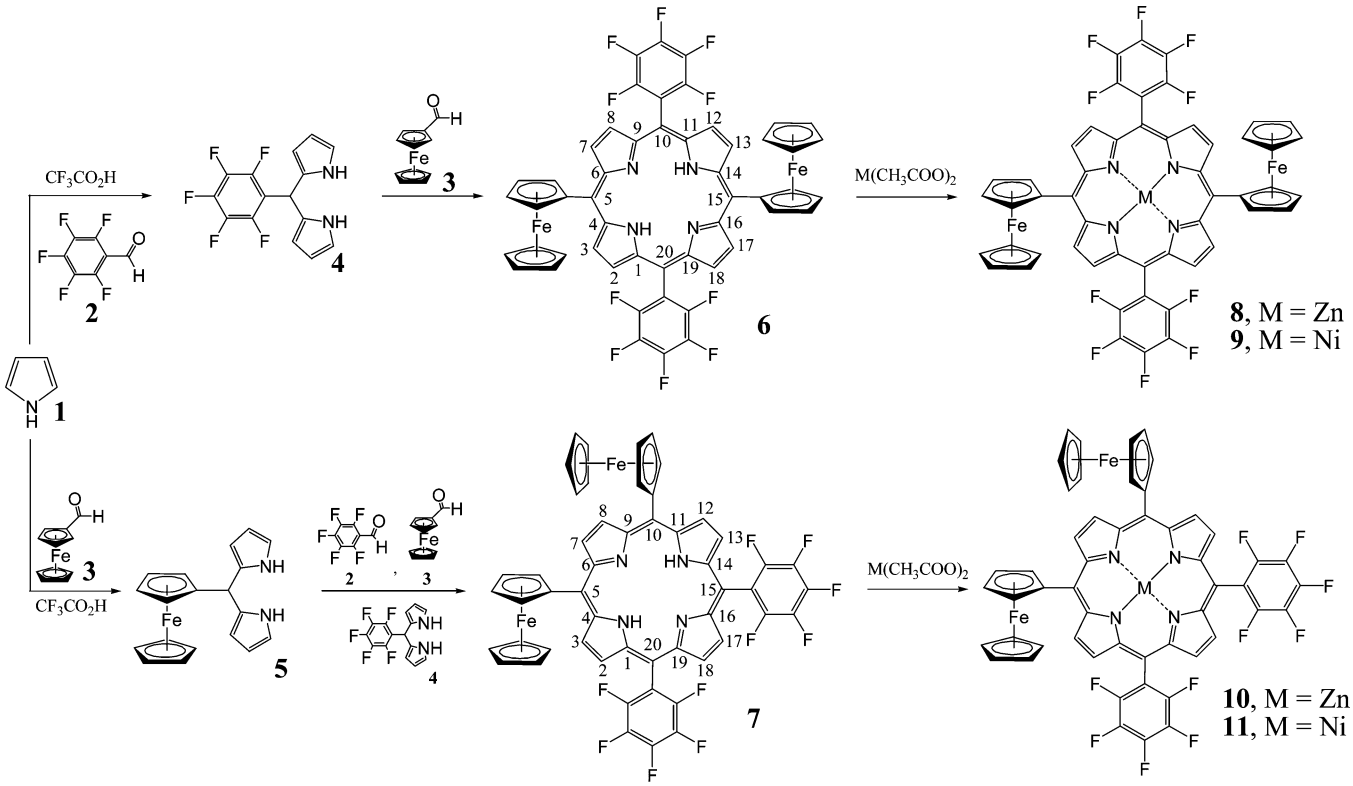

substituted porphyrins bearing simultaneously electron-donating ferrocenyl and electron-withdrawing fluorine substituents may have interesting new chemical, electrochemical, and other physical properties. A key aspect in studies involving porphyrins with different substituents is the selective synthesis, isolation, and characterization of single isomers from mixtures of different substituted macrocycles.[16] A need clearly exists to develop the chemistry surrounding porphyrin complexes bearing multiple substituent types, including those having simultaneously electron-withdrawing and electron-donating substituents. Consequently, in this publication, we report the synthesis and electronic and electrochemical properties of symmetrically *and* unsymmetrically substituted porphyrin isomers bearing simultaneously two-electron-withdrawing pentafluorophenyl and two-electron-donating ferrocenyl groups.[17]

Results and Discussion

Synthesis. The overall synthetic route to the target porphyrins of this study is illustrated in Scheme 1. The reaction of pyrrole, **1**, with 2,3,4,5,6-pentafluorobenzaldehyde, **2**, or ferrocenecarboxaldehyde, **3**, gave respectively, after addition of a catalytic amount of trifluoroacetic acid and chromatographic purification, dipyrromethanes **4** (29% yield) and **5** (77% yield). The high-yield synthesis of **5**, which decomposed faster in solution when exposed to a normal air atmosphere, was also described elsewhere[18] and is considered the result of the presence of the strong electron-donating ferrocenyl group.

The porphyrins **6** and **7** are structural isomers of each other. In porphyrin **6**, the *meso*-substituted ferrocenyl groups are in positions 5 and 15. We label this structural isomer the *trans* isomer. In the case of isomer **7**, the ferrocenyl units are situated in the 5 and 10 *meso* positions, and this conformation is referred to as the *cis* structural isomer.

Porphyrins bearing two different substituents in the *meso* positions (*trans*-A_2B_2 or *cis*-A_2B_2) have been available via a statistical condensation of pyrrole **1** with two different aldehydes, e.g., **2** and **3**.[18,19] However, the synthesis of the present ferrocene-containing porphyrins **6** and **7** involved higher yielding condensations of dipyrromethanes with suitable aldehydes. The *trans* isomer **6** was obtained by reacting ferrocenecarboxaldehyde, **3**, with the dipyrromethane **4**, under Schlenck conditions, following Lindsey protocols.[20] To fully aromatize the porphyrinoid species that formed, the reaction was quenched with an excess of DDQ (2,3-dichloro-5,6-dicyanobenzoquinone).

A different route was considered for the preparation of the *cis* isomer, **7**. It involved the simultaneous mixed condensation of equimolar amounts of dipyrromethanes **4** and **5** with aldehydes **2** and **3**. Chromatographic separation rid **7** of different porphyrin compounds and other byproducts. Porphyrin **7** was isolated in 4% yield and was characterized by elemental analysis as well as with various spectroscopic methods. The poor yield of **7** (4%) as compared to the yield for **6** (22%) is explained by noting that, statistically, the cyclocondensation to obtain **7** can lead to more porphyrin products with different *meso* substituent patterns (e.g., AAAA, AAAB, ABAB, or ABBB) than in the case of **6**.

Metalation of **6** and **7** with zinc acetate or nickel acetate was done in DMF (*N*,*N*-dimethylformamide). High-yield formations of the zinc derivatives **8** (76%) and **10** (93%) and nickel

(16) Bonnett, R. *Chem. Rev.* **1995**, *24*, 19.

(17) After this study was completed we also became aware of novel work performed by Gryko in this area; Koszarna, B.; Butenschön, H.; Gryko, D. T. *Org. Biol. Chem.* **2005**, *3*, 2640.

(18) Gallagher, J. F.; Moriarty, E. *Acta Crystallogr., Sect. C: Cryst. Struct. Commun.* **1999**, *55*, 1079.

(19) Littler, B. J.; Miller, M. A.; Hung, C.; Wagner, R. W.; O'Shea, D. F.; Boyle, P. D.; Lindsey, J. S. *J. Org. Chem.* **1999**, *64*, 1391

(20) (a) Lindsey, J. S. In *The Porphyrin Handbook*; Kadish, K. M., Smith, K. M., Guilard, R., Eds.; Academic Press: New York, 2000; Vol. 1, p. 45. (b) Rao, P. D.; Dhanalekshmi, S.; Littler, B. J.; Lindsey, J. S. *J. Org. Chem.* **2000**, *65*, 7323.

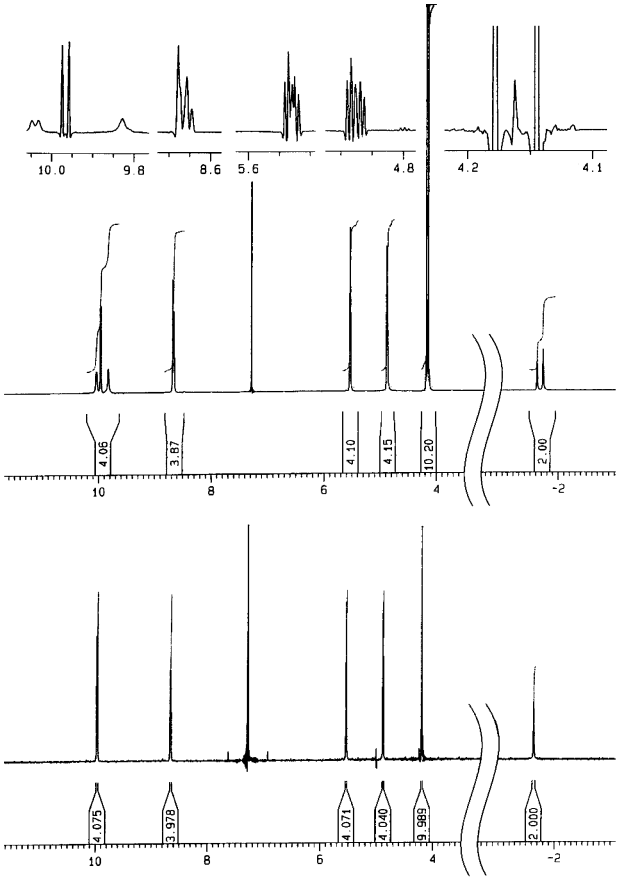

Figure 1. ^{1}H NMR spectra of porphyrins **6** (bottom) and **7** (middle and top).

derivatives **9** and **11** (62% and 57%, respectively) were observed. The new porphyrins **6**−**11** are all stable in air and are soluble in common organic solvents.

^{1}H NMR Spectroscopy. ^{1}H NMR characterization distinguished conclusively between the *trans* conformational isomer **6** and the *cis* conformational isomer **7**. The room-temperature ^{1}H NMR spectrum obtained for **6** in $CDCl_3$ (Figure 1) showed a simple pattern in the aromatic region. Two doublets at 9.97 and 8.66 ppm integrated for four protons each and were assigned to two sets of β-pyrrolic protons. This reflects perfectly the *trans*-A_2B_2 symmetry of the isomer **6**. The electron-withdrawing effect of the pentafluorophenyl groups through the π-conjugated system of the porphyrin core is believed to deshield the β-pyrrolic protons adjacent to the pentafluorophenyl groups and results in the low-field chemical shift peak position of 9.97 ppm. Inversely, the electron-donating effect of the ferrocenyl groups shields the β-pyrrolic protons adjacent to the ferrocenyl groups, causing the resonance peak to be at the high-field position of 8.66 ppm. The zinc derivative of **6**, namely, porphyrin **8**, exhibited a similar ^{1}H NMR spectrum in this region. However, the two pyrrolic doublet signals were observed at the relatively more downfield positions of 10.21 and 8.86 ppm, respectively. In contrast, the signals associated with the β-pyrrolic protons of the nickel porphyrin derivative **9** appeared at 9.64 and 8.52 ppm. These observations can be related to the *cationic* electronegativities, $\chi_{(cat)n+}$ of the coordinating metallic cations. Zinc cations ($\chi_{Zn2+} = 1.1$) are less electronegative than nickel cations ($\chi_{Ni2+} = 2.00$).[21] This implies that the Ni^{2+} cation withdraws more electron density from the porphyrin ring, causing its β-pyrrole proton peak positions to appear at much higher field than does the zinc derivative. The zinc cation is so weakly electronegative that it enriches electron density on the porphyrin macrocycle compared to both the Ni porphyrin and the 2H porphyrin. On the assumption that there is a linear relationship between pyrrole ^{1}H NMR peak positions and cation electronegativity, it follows that the electronegativity of the proton pair should be ca. $\chi_{2(H+)} = 1.5-1.6$. This value is very much substantiated by the Soret band λ_{max} electronic spectra results (see below) and differs by 0.5−0.6 units from the atomic Pauling $\chi_H = 2.1$ value.

The pyrrole chemical shifts and ^{1}H NMR signal patterns recorded for the *cis* isomer **7** were more complex. Rather than two clean doublets, multiple ^{1}H NMR signals for the eight β-pyrrolic protons were observed (Figure 1). Two nearly overlapping doublets that integrated for four protons were observed at 8.65 ppm. Further downfield, a multiplet at 9.83 ppm (for 1H) and two doublets at 9.97 (for 2H) and 10.05 ppm (for 1H) were observed. This rather unusual pattern may be associated with atropisomerism resulting from the presence of two ferrocenyl units in the 5 and 10-*meso* positions. Also, restricted rotation of the ferrocenyl groups by virtue of their close proximity could influence the electronic environments of the number 7 and 8 β-pyrrolic protons located between these organometallic substituents. It is important to notice that, so far, ^{1}H NMR spectroscopy was the only method that could distinguish **6** from **7**. Since their molecular weight as well as molecular formulas are identical due to their isomeric relationship (Scheme 1), their mass spectra and elemental analyses data were the same. Further upfield in the spectra, the typical signals of monosubstituted ferrocenyl units were in agreement with the *trans* and *cis* substitution patterns of **6** and **7**. Chemical shifts and multiplicity of signals at 5.54 (t), 4.89 (t), and 4.21 (s) ppm for **6** are in agreement with freely rotating ferrocenyl groups in the 5 and 15 *meso* positions. The ^{1}H NMR signals of the ferrocenyl group of **7** were recorded at 5.54 (m), 4.88 (m), and 4.16 (two singlets). The multiplicity of these signals, Figure 1, is again consistent with a *cis* 5,10-ferrocenyl substitution pattern that invokes restricted rotation. ^{1}H NMR data for **10** and **11** also clearly differentiated the *cis* zinc and nickel derivatives, different from the corresponding *trans* analogues; data are presented in the Experimental Section.

The ferrocenyl-based ^{1}H NMR signals of the zinc derivatives **8** and **10** and nickel derivatives **9** and **11** were observed at almost the same chemical shifts as were recorded for **6** and **7**, indicating the Zn^{2+} and Ni^{2+} metal cation centers did not transmit their relative electronic effects to *meso* substituents as effectively as they do to the β-pyrrole positions.

Furthermore, the chemical shifts for the imino (NH) protons of **6** and **7** were observed as two overlapping singlets at −1.66 ppm (for **6**) and as two separate singlets at −1.63 and −1.73 ppm for **7**, respectively. The presence of two ferrocenyl units adjacent to each other at the 5 and 10-*meso* positions of **7** implies that the two inner imino protons of isomer **7** are magnetically nonequivalent and therefore that the two inner imino protons are situated in different chemical environments. No signal assignable to any NH protons was observed in the case of **8**−**11**, providing further evidence for the elemental analyses of the successful insertion of metal cations in the macrocyclic cavities of **8** and **10** (Zn^{2+}) and **9** and **11** (Ni^{2+}).

Electronic Absorption Spectroscopy. Porphyrins **6**−**11** are dark purple in the solid state but have a greenish tint in solution. As demonstrated in Figure 2, the electronic spectra of porphyrins **6**−**11** in THF all exhibited the characteristic strong Soret band

(21) Duffy, A. *J. Chem. Soc., Dalton Trans.* **1983,** 1475.

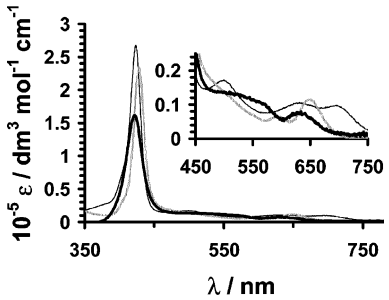

Figure 2. Electronic spectra of porphyrins **6** (thin black line, 2.17 × 10^{-6} M), **8** (bold gray line, 2.23 × 10^{-6} M), and **9** (bold black line, 7.49 × 10^{-7} M) in THF. The inset highlights the Q-band region.

in the 400−450 nm region. The spectra of the free base porphyrins **6** and **7** (not shown) overlapped almost exactly. They both showed the intense Soret maximum at 424 nm and a shoulder at 496 nm. The Q-bands featured two peaks very close to each other at 631 (Q_x) and 697 nm (Q_y). Two-fold degeneracy of the lowest energy singlet state of the metal-free derivatives **6** and **7** explains the splitting of the Q-band. The spectra of **8** and **10** (not shown) and **9** and **11** (not shown) overlapped also almost exactly. The zinc-metalated derivatives **8** and **10** exhibited a red-shifted Soret band with peak maxima at 428 nm compared to the free base **6**. A blue-shifted Soret band with peak maxima at 421 nm was observed for the nickel complexes **9** and **11**. It is also apparent that by introducing a metal in the cavity of **6** (or **7**) the Soret band extinction coefficient was reduced significantly (Figure 2). Lower extinction coefficients are consistent with stronger aggregation of metalated porphyrins in the absence of axial ligation. Upon comparing Soret band maxima of **6** with that of 5,10,15,20-tetraphenylporphyrin (2Htpp), porphyrin **6** exhibits a red-shift in the Soret band maxima from 416 to 424 nm. This may be rationalized in terms of the sum of group electronegativities, χ_{tot}, of the combined *meso* substituents. Since $\chi_{Fc} = 1.87$[12] and $\chi_{C6F5} = 2.46$,[22] $\chi_{tot,\mathbf{6}} = 8.66$ on the Gordy scale. For 2Htpp, having four *meso*-substituted phenyl groups ($\chi_{C6H5} = 2.21$[12]), $\chi_{tot} = 8.84$. It follows that the macrocyclic core of **6** and **7** should be *more* electron rich than that of 2Htpp, because the combined group electronegativity of the *meso* substituents of **6** and **7** is 0.22 Gordy scale units less than for 2Htpp. This translates to a longer wavelength Soret band λ_{max} value for **6** than for 2Htpp. That longer λ_{max} values are linearly associated with smaller group electronegativity values, i.e., more electron-rich species, was also observed for the ν(CO) stretching frequency wave numbers of [Rh(β-diketonato)(CO)(PPh_3)] complexes[23] ($\nu = 10^7/\lambda$ with λ in nm, ν in cm^{-1} units) and for the ν(C═O) stretching frequencies of methyl esters of the type RCOOMe.[24] Following the [Rh(β-diketonato)(CO)(PPh_3)] and RCOOMe queue, a linear relationship between λ_{max} and $\chi_{cations}$ of **8** and **9** was assumed, and it led upon extrapolation to $\chi_{2(H+)} = 1.5$ for the free base porphyrin **6**. This value is mutually consistent with that obtained from the ^{1}H NMR β-pyrrole peak position/$\chi_{cations}$ relationship described above.

Electrochemistry. Cyclic voltammetry (CV) experiments were conducted in dry CH_2Cl_2 utilizing 0.1 mol dm^{-3} [NBu_4][$B(C_6F_5)_4$] as supporting electrolyte in order to restrict any solvent/porphyrin or electrolyte/porphyrin ion-pairing interactions to a minimum.[25] Electrochemical data are summarized in Table 1. Cited potentials are corrected to be referenced against Fc/Fc^+, as required by IUPAC.[26] Experimentally, to prevent signal overlapping, decamethylferrocene (Fc*) was used as internal reference. Under our conditions, the $(Fc^*)/(Fc^*)^+$ couple was found to be at −610 mV versus Fc/Fc^+. Electrochemical reversibility for one-electron-transfer processes at 25 °C is characterized by peak potential differences of $E_{pa} - E_{pc} = \Delta E_p = 59$ mV (pa = peak anodic, pc = peak cathodic) and is independent of the scan rate.[27] Because under our experimental conditions decamethylferrocene exhibited an experimentally determined ΔE_p value of 78 mV and ferrocene itself gave $\Delta E_p = 81$ mV, within the context of this paper, experimentally determined ΔE_p values smaller than 90 mV are considered to imply electrochemically reversible behavior. Larger ΔE_p values are considered to represent electrochemically quasi-reversible behavior (Table 1).

Compounds **6**−**11** showed two ring-centered one-electron-transfer reduction waves labeled 1 and 2 in Figures 3 and 4, two ferrocenyl substituent one-electron-transfer oxidation waves labeled 3 and 4, and one ring-centered one-electron-transfer oxidation wave labeled 5 within the potential window that CH_2Cl_2 as solvent allows. 2Htpp exhibited a second ring-centered one-electron oxidation process in the CH_2Cl_2 potential window, and this process is labeled 6 in the CV shown in Figure 4. Except for wave 1 for the nickel complexes **9** and **11**, waves 1 and 6 for 2Htpp, and wave 5 for the *cis* complexes **10** and **11**, every electron-transfer process was electrochemically reversible, with $\Delta E_p < 90$ mV at scan rate 100 mV s^{-1} (Table 1). Chemical reversibility was good with peak current ratios (calculated as the current of the reverse scan divided by the current of the forward scan) approaching 1 for all processes except those associated with wave 6 of 2Htpp, wave 1 for the nickel complex **9**, and wave 5 for complexes **6**−**11**. The general current ratio deviation from unity of wave 5 is consistent with a weak onset of electrode pollution, probably via electrode deposition after the formation of the poorly soluble, doubly charged [$M(Fc^+)_2$Por] species during wave 4 (Figures 3 and 4). It will also explain the prewave sometimes observed at wave 5. Re-reduction at wave 4 must redissolve any precipitated material from the electrode surface, as wave 4 has very reversible characteristics.

Linear sweep voltammetry (LSV) confirmed waves 1−6 are all involved in processes where the same amount of electrons (one electron) is transferred. Figure 3 demonstrates this for **6**. The partially resolved peaks 3 and 4 assigned to the two ferrocenyl substituents were much better resolved by Osteryoung square wave voltammetry. This is also demonstrated in Figure 3 for **6**. The use of the extreme noninteracting CH_2Cl_2/0.1 mol dm^{-3} [$N(^nBu_4)$][$B(C_6F_5)_4$] solvent electrolyte system[28] minimized ion pairing to the point that the two ferrocene waves did not coalesce but became resolved. Repetition of the CV experiment of **6**, in the coordinating solvent acetonitrile using the traditional [$N(^nBu_4)$][PF_6] electrolyte, resulted in two strongly overlapping ferrocene-based electrochemical waves, which could not be resolved at all. Different formal reduction potentials for side groups on symmetrical complexes in which mixed-valent

(22) Swarts, J. C.; Erasmus, E. Unpublished results.

(23) Conradie, J.; Lamprecht, G. J.; Otto, S.; Swarts, J. C. *Inorg. Chim. Acta* **2002**, *328*, 191.

(24) Kagarisa, R. E. *J. Am. Chem. Soc.* **1955,** *77*, 1377.

(25) Barriere, F.; Kirss, R. U.; Geiger, W. E. *Organometallics* **2005**, *24*, 48, and references therein.

(26) Gritzner, G.; Kuta, J. *Pure Appl. Chem.* **1984**, *56*, 461.

(27) (a) Evans, D. H.; O'Connell, K, M.; Peterson, R. A.; Kelly, M. J. *J. Chem. Educ.* **1983**, *60*, 291. (b) Kissinger, P. T.; Heineman, W. R. *J. Chem. Educ.* **1983**, *60*, 702. (c) Van Benshoten, J. J.; Lewis, J. Y.; Heineman, W. R. *J. Chem. Educ.* **1983**, *60*, 772. (d) Sawyer, T.; Roberts, J. L. In *Experimental Electrochemistry for Chemists*; John Wiley and Sons: New York, 1974; p 118.

(28) Barriere, F.; Geiger, W. E. *J. Am. Chem. Soc.* **2006**, *128*, 3980.

Table 1. Cyclic Voltammetry Data (potentials vs Fc/Fc^+, scan rate = 100 mV s^{-1}) of 1.0 mmol dm^{-3} Solutions of Analytes in CH_2Cl_2 Solutions Containing 0.1 mol dm^{-3} $[N(^nBu)_4][B(C_6H_5)_4]$ at 25 °C

wave	E_{pc}/V	ΔE_p/mV	$E^{o'}$/V	$i_{pc}/\mu A$	i_{pc}/i_{pa}	wave	E_{pc}/V	ΔE_p/mV	$E^{o'}$/V	$i_{pc}/\mu A$	i_{pc}/i_{pa}
		Ferrocene						2Htpp			
---	-0.040	80	0.000	6.08	0.96	**1**	-2.120	99	-2.071	3.90	0.97[a]
		Decamethylferrocene				**2**	-1.796	82	-1.755	3.21	0.99[a]
---	-649	78	-0.610	3.90	0.94	**5**	0.417	79	0.452	3.04[b]	0.86[b]
						6	0.850	148	0.924	1.03	0.59[d]
		2HPtrans, **6**						2HPcis, **7**			
1	-1.962	79	-1.923	2.35	0.96[a]	**1**	-1.960	86	-1.917	2.87	0.96[a]
2	-1.601	74	-1.564	2.63	0.96[a]	**2**	-1.604	77	-1.566	2.43	0.97[a]
3	0.063	70	0.098	2.50	0.93	**3**	0.070	60	0.100	2.98	0.95
4	0.174	70	0.209	2.50	0.95	**4**	0.178	74	0.215	2.87	0.98
5	1.128	77	1.167	1.84	0.67[c,d]	**5**	1.123	81	1.164	1.85	0.62[c,d]
		ZnPtrans, **8**						ZnPcis, **10**			
1	-2.152	85	-2.110	2.61	0.94[a]	**1**	-2.165	110	-2.110	2.26	0.98[a]
2	-1.759	72	-1.723	2.78	0.96[a]	**2**	-1.798	119	-1.739	2.51	0.95[a]
3	0.027	79	0.067	2.85	0.92	**3**	0.023	88	0.067	2.33	0.96
4	0.130	70	0.169	2.74	0.95	**4**	0.127	86	0.170	2.26	0.96
5	0.921	73	0.958	2.53	0.72[c,d]	**5**	0.852	144	0.924	1.47	0.63[d]
		NiPtrans, **9**						NiPcis, **11**			
1	-2.236	109	-2.182	1.60	0.78[a,]	**1**	-2.225	114	-2.168	2.40	0.97[a]
2	-1.744	86	-1.701	1.69	0.98[a]	**2**	-1.759	91	-1.714	2.17	0.95[a]
3	0.077	60	0.107	1.65	0.94	**3**	0.058	78	0.097	2.36	0.99
4	0.184	64	0.216	1.79	0.95	**4**	0.154	86	0.192	2.26	0.98
5	1.069	77	1.108	1.43	0.62[c,d]	**5**	0.927	199	1.126	1.12	0.35[c,d]

[a] i_{pa}/i_{pc} [b] When the switching potential is chosen to exclude wave 6 from the scan, $i_{pc}/i_{pa} = 0.96$ [c] Approximate value, the weak shoulder directly before wave 5 causes baseline uncertainty [d] Slow electron-transfer kinetics and/or electrode deposition distorts this value.

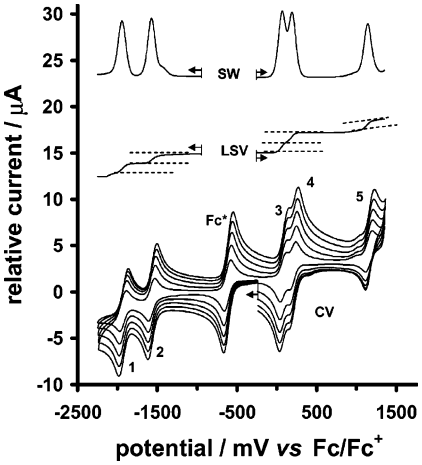

Figure 3. Top: Osteryoung square wave voltammogram of 1 mmol dm^{-3} solutions of **6** in dichloromethane containing 0.1 mol dm^{-3} $[N(^nBu)_4][B(C_6F_5)_4]$ at 10 Hz and 25 °C. Middle: Linear sweep voltammetry at 2 mV s^{-1}. Bottom: Cyclic voltammograms of **6** in dichloromethane at a scan rate of 100, 200, 300, 400, and 500 mV s^{-1} on a glassy-carbon working electrode. The peak labeled Fc* is that of decamethylferrocene, which has been added as an internal standard to the solution. The prewave before wave 5 is commented on in Figure 4.

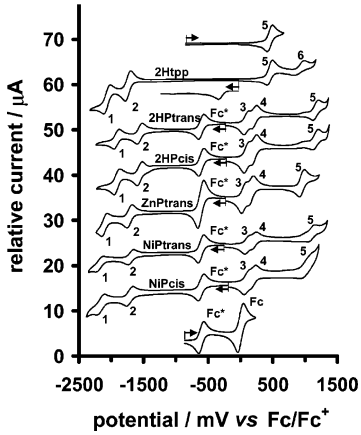

Figure 4. Cyclic voltamogramms of 1 mmol dm^{-3} solutions of (in order from bottom to top) ferrocene (Fc) and decamethylferrocene (Fc*), **11** (NiPcis), **9** (NiPtrans), **8** (ZnPtrans), **7** (2HPcis), **6** (2HPtrans), 2Htpp, and 2Htpp scanned over the limited potential range of −0.80 to 0.70 V in dichloromethane containing 0.1 mol dm^{-3} $[N(^nBu)_4][B(C_6F_5)_4]$ at 25 °C at a scan rate of 100 mV s^{-1} on a glassy-carbon working electrode. The prewaves before wave 5 for the 2H and Ni derivatives are not due to an impurity. They probably arise from electrode pollution (deposition) after the formation of the poorly soluble doubly charged $[M(Fc^+)_2Por]$ species during wave 4. Inset: Below the 2Htpp scan is a blowup of this scan showing clearly the peak at −331 mV, which is linked to wave 6. As the top CV shows, this peak is absent when the turn-around potential excludes wave 6.

intermediates are generated are well known in systems that allow electron delocalization, either through intramolecular through-bond paths or from a direct metal−metal interaction.[29,30] Both the aromatic porphyrinoid core and the ferrocenyl side groups allow delocalization of electrons, and the ease at which multiferrocenyl systems generate mixed-valent intermediates has been described prior to this work by our research group.[31] The inequivalence of the ferrocenyl and ferrocenium groups of the mixed-valent intermediates of **6**−**11** are highlighted in terms of the group electronegativities, $\chi_{Fc} = 1.87$[12,30] and $\chi_{Fc+} = 2.82$.[31,32] The electron-withdrawing power of the ferrocenium group is almost as high as that of the CF_3 group ($\chi_{CF3} = 3.01$).[12,31]

(29) (a) Creutz, C.; Taube, H. *J. Am. Chem. Soc.* **1969**, *91*, 3988. (b) Geiger, W. E.; Van Order, N.; Pierce, D. T.; Bitterwolf, T. E.; Reingold, A. L.; Chasteen, N. D. *Organometallics* **1991**, *10*, 2403. (c) Van Order, N.; Geiger, W. E.; Bitterwolf, T. E.; Reingold, A. L. *J. Am. Chem. Soc.* **1987**, *109*, 5680. (d) Pierce, D. T.; Geiger, W. E. *Inorg. Chem.* **1994**, *33*, 373.

(30) Conradie, J.; Cameron, T. S.; Aquino, M. A. S.; Lamprecht, G. J.; Swarts, J. C. *Inorg. Chim. Acta* **2005**, *358*, 2530.

(31) Du Plessis, W. C.; Erasmus, J. J. C; Lamprecht, G. J.; Conradie, J.; Cameron, T. S.; Aquino, M. A. S.; Swarts, J. C. *Can. J. Chem.* **1999**, *77*, 378.

Scheme 2. Ring-Based and Ferrocenyl Group Electron-Transfer Reactions Associated with Redox Potentials for Compounds 6−11 and 2Htpp

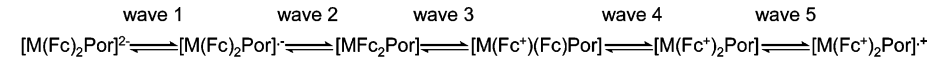

2Htpp	-2.071	-1.755	-	-	0.452
2HPtrans (**6**)	-1.923	-1.564	0.098	0.209	1.167
2HPcis (**7**)	-1.917	-1.566	0.100	0.215	1.164
ZnPtrans (**8**)	-2.110	-1.723	0.067	0.169	0.958
ZnPcis (**10**)	-2.110	-1.739	0.067	0.170	0.924
NiPtrans (**9**)	-2.182	-1.701	0.107	0.216	1.108
NiPcis (**11**)	-2.168	-1.714	0.097	0.192	1.126

The individual electron-transfer reactions associated with waves 1−6 in Figures 3 and 4 are assigned in Scheme 2. Inspection of the formal reduction potentials, $E^{\circ\prime} = 1/2(E_{pa} + E_{pc})$, associated with these potentials reveal two key factors emanating from this study.

The first is associated with the observation that $E^{\circ\prime}$ of peak 1 of the zinc and nickel complexes is smaller (i.e., more negative) than that of 2Htpp (Figure 4). This is interpreted as a consequence of $\chi_{tot} = 8.84$ for the four phenyl substituents in 2Htpp being 0.22 Gordy eletronegativity units larger than $\chi_{tot} = 8.66$ for the two C_6F_5 and two ferrocenyl *meso* substituents of **8**−**11**. These χ_{tot} values show **8**−**11** should be more electron rich than 2Htpp and therefore slightly easier to reduce. Peak 2 does not follow this trend unambiguously, as **8**−**11** and 2Htpp have comparable $E^{\circ\prime}$ values. In contrast, oxidation wave 5 for the zinc and nickel complexes **8**−**11** as well as for the free base complexes **6** and **7** are found at $E^{\circ\prime}$ potentials 0.5−0.7 V larger than for 2Htpp. This striking difference is easily explained upon recognizing that the ferrocenyl groups have been oxidized to the ferrocenium species with $\chi_{Fc+} = 2.82$ at waves 3 and 4. This changes the combined substituent group electronegativities for **6**−**9** at wave 5 to $\chi_{tot} = 10.56$. This large χ_{tot} value implies that **6**−**11** are much more electron poor and therefore more difficult to oxidize than 2Htpp at potentials associated with the redox processes of wave 5. The introduction of redox-tuneable side chains to porphyrins **6**−**11** therefore led to the unusual result that ring-centered reductions occur in electron-rich macrocycles, but ring-centered oxidations occur in electron-deficient species.

The second key point that can be quantified from the observed formal reduction potentials relates to the relative electronic influence of the Zn^{2+}, Ni^{2+}, and $2(H^+)$ centers. The relatively higher cation electronegativity of Ni^{2+} over Zn^{2+} ($\chi_{Zn2+} = 1.1$, $\chi_{Ni2+} = 2.0$) implies that **8** (and **10**) has a higher ring-centered electron density than **9** and **11**. This implies that $E^{\circ\prime}$ for all couples of **8** and **10** should be observed at lower potentials than for **9** and **11.** Experimentally this was verified for couples 2−5 (Scheme 2). The failure of wave 1 to follow this trend may be related to the electrochemical irreversibility of wave 1 of complexes **9** and **11** ($\Delta E = 109$ and 114 mV, respectively), or alternatively, the degree of ruffling for the doubly reduced Ni complexes may be different from that of the other complexes. Additionally, the ^{1}H NMR and electronic spectra-derived $2(H^+)$ electronegativity of $\chi_{2(H+)} = 1.5-1.6$ would imply that complexes **6** and **7** should have $E^{\circ\prime}$ values intermittently between that of **8**−**11** in the resting state, i.e., at redox processes associated with waves 2 and 3. In practice this was only marginally observed for wave 3, where electron-transfer did not change the redox state of the macrocycle itself, but that of a substituent. In addition, while the zinc complexes **8** and **10** did show the expected lower $E^{\circ\prime}$ values compared to **6** and **7** for all five redox steps, $E^{\circ\prime}$ values for waves 1, 2, and 5 of the nickel complexes were lower rather than higher compared to the corresponding waves of **6** and **7**. The deviation from the expected pattern relating to waves 1 and 5 of the Ni complexes is in part attributed to the fact that some of these couples are not electrochemically reversible ($\Delta E_p \geq 100$ mV), implying that the indicated $E^{\circ\prime}$ values are not true thermodynamic quantities. Electrode deposition of oxidized products associated especially with wave 4 may also play a role. Different degrees of ruffling for the Ni complexes compared to that of the other complexes upon redox reactions may also contribute to lower than expected reduction potentials. The fact that the macrocycles are only for waves 3 and 4 in the same redox state, namely, $(porphyrin)^{2-}$, than for the ^{1}H NMR and the electronic spectroscopy study, must also contribute to the observed deviations.

With respect to 2Htpp, oxidation waves 5 and 6 introduced interesting features in the present solvent electrolyte system. Oxidation of the [MPor] species to $[MPor]^{\bullet+}$ at wave 5 happened smoothly, but the reduction half-wave associated with the reaction $[MPor]^{\bullet+} \rightarrow [MPor]$ was less intense than expected (i_{pc} current values are small, $i_{pc}/i_{pa} = 0.86$). During the cathodic cycle, a new reduction wave appeared at −331 mV (Figure 4, blowup under CV second from the top). However, when the switching potential during the positive scan was lowered from 1.3 V to 0.6 V, i.e., when wave 6 was not engaged during the CV cycle, wave 5 had the characteristic CV appearance with $\Delta E_p = 87$ mV and $i_{pc}/i_{pa} = 0.96$, and the new peak at −331 mV was absent (Figure 4, top). It follows that the species that leads to the new peak at −331 mV must be the oxidized species generated at wave 6, namely, a follow-up product of $[MPor]^{2+}$. Wave 6 is associated with the $[MPor]^{\bullet+}/[MPor]^{2+}$ redox system and represents a chemically and electrochemically irreversible process because $\Delta E_p \approx 148$ mV and $i_{pc}/i_{pa} = 0.59$. Electrode deposition and enhanced aggregation of the doubly charged $[MPor]^{2+}$ species in CH_2Cl_2 are the most probable causes of this behavior. The process leading to the new wave at −331 mV partially removes material from the bilayer next to the electrode, which would account for the lower than expected $i_{pc}/i_{pa} = 0.86$ ratio for wave 5. At slow scan rates, the peak at −331 mV was very weak, but it became stronger at fast scan rates.

Conclusion

In summary, new porphyrin isomers **6**−**11** substituted by two ferrocenyl units and two pentafluorophenyl units were synthesized and fully characterized. The rich electrochemistry of these new complexes was found to be strongly dependent on the group electronegativity of the pentafluorophenyl and ferrocenyl substituents and also of the cationic electronegativity of the central metallic cation M^{n+} coordinated in the porphyrin cavity. To our knowledge, porphyrin formal reduction potentials were for the first time quantitatively placed in perspective utilizing group and cationic electronegativities. In addition, the introduction of

(32) Davis, W. L.; Shago, R. F.; Langner, E. H. G.; Swarts, J. C. *Polyhedron* **2005**, *24*, 1611.

redox-tuneable side chains led to the unusual result that ring-centered porphyrin reductions occur in electron-rich macrocycles, but ring-centered oxidations occur in electron-deficient macrocycles. The potential use of these complexes as second-generation photosensitisers is now under investigation.

Experimental Section

General Procedures. Solid reagents and liquid reactants except pyrrole (Merck or Aldrich) were used without further purification. Solvents were distilled prior to use, and water was double distilled. Pyrrole was distilled from CaH_2 under argon. All reactions required anhydrous conditions and were therefore conducted under a nitrogen atmosphere. $[N(^nBu)_4][B(C_6F_5)_4]$ was synthesized according to published procedures.[33]

Column chromatography was performed on silica gel 60 (particle size 0.040−0.063 mm). ^{1}H NMR spectra were recorded on a Bruker Advance DPX 300 NMR spectrometer (300 MHz) in $CDCl_3$ solutions. Chemical shifts are reported relative to $SiMe_4$ at 0 ppm. UV/vis spectra were recorded on a Cary 50 probe UV/visible spectrophotometer. Elemental analyses were performed by the Canadian Microanalytical Service Ltd., Canada.

5-(Pentafluorophenyl)dipyrromethane (4). The procedure is a modification of that described in ref 19. A solution of 2,3,4,5,6-pentafluorobenzaldehyde (0.70 g, 3.60 mmol) and pyrrole (10 mL, 0.144 mol, 40 equiv) was degassed by bubbling nitrogen for 10 min before trifluoroacetic acid (0.026 mL, 0.36 mmol) was added. The solution was stirred at room temperature for 15 min in the dark, diluted with DCM (2 × 100 mL), washed with 0.1 M NaOH (100 mL), and dried over magnesium sulfate. Solvents and the excess of pyrrole were removed under reduced pressure. Purification of the resulting slurry by column chromatography over silica (eluent cyclohexane/EtOAc/triethylamine, 80:20:1) gave 5-(pentafluorophenyl)dipyrromethane, **4** (0.32 g, 29%), as a colorless solid; mp 110 °C (lit. mp 110−112 °C);[19] δ_H (300 MHz, $CDCl_3$) 8.06 (2H, br s, NH), 6.73 (2H, m), 6.22 (2H, m), 6.11 (2H, m), 5.93 (1H, s).

5-Ferrocenyldipyrromethane (5). A sample of ferrocenecarboxaldehyde (0.75 g, 3.50 mmol) was treated as described in the procedure for **4**, affording 5-ferrocenyldipyrromethane (0.88 g, 77%) as a yellow powder; mp 130−131 °C (lit. 131−132 °C);[18] δ_H (300 MHz, $CDCl_3$) 8.00 (2H, br s, NH), 6.79 (2H, m), 6.18 (2H, m), 6.02 (2H, m), 5.22 (1H, s), 4.19 (2H, m), 4.09 (7H, m).

5,15-Bisferrocenyl-10,20-bis(pentafluorophenyl)porphyrin (6). Ferrocenecarboxaldehyde (137 mg, 0.64 mmol) and 5-(pentafluorophenyl)dipyrromethane (200 mg, 0.64 mmol) were dissolved in DCM (100 mL) at room temperature in the dark before trifluoroacetic acid (3 mg, 0.025 mmol) was added to initiate the condensation. After the mixture was stirred for 15 h at room temperature, the reaction was quenched with DDQ (0.22 g, 0.96 mmol). Stirring continued for 1 h before triethylamine (2.5 mg, 0.025 mmol) was added to neutralize the acid. The solvents were removed under reduced pressure, and the resultant material was purified by column chromatography over silica (eluent: hexane/DCM, 1:1) to give a sticky purple solid. The crude product was triturated with methanol and filtered off to afford 5,15-bisferrocenyl-10,20-bis(pentafluorophenyl)porphyrin, **6** (70 mg, 22%), as a purple powder, mp >200 °C. Anal. Found: C, 61.75; H, 2.84; N, 5.70. $C_{52}H_{28}N_4F_{10}Fe_2$ requires C, 61.80; H, 2.79; N, 5.54. δ_H (300 MHz, $CDCl_3$) 9.97 (4H, d, *J* 5), 8.66 (4H, d, *J* 5), 5.54 (4H, m), 4.89 (4H, m), 4.21 (10H, s), −1.66 (2H, s); λ_{max} (2.17×10^{-6} M in THF) 423 ($\epsilon = 2.76 \times 10^5$) nm.

5,10-Bisferrocenyl-15,20-bis(pentafluorophenyl)porphyrin (7). Ferrocenecarboxaldehyde (214 mg, 1.00 mmol), 5-(pentafluorophenyl)dipyrromethane (312 mg, 1.00 mmol), 5-ferrocenyldipyrromethane (330 mg, 1.00 mmol), and 2,3,4,5,6-pentafluorobenzaldehyde (196 mg, 1.00 mmol) were dissolved in DCM (400 mL) at room temperature before trifluoroacetic acid (1.14 g, 10.00 mmol) was added. After 15 h of stirring at room temperature, DDQ was added (0.34 g, 1.50 mmol). Stirring continued for an additional hour before purification by column chromatography over silica gave three fractions. The first fraction (eluent hexane/DCM, 2:1) contained the 5-ferrocenyl-10,15,20-tris(pentafluorophenyl)porphyrin (10 mg, 1%); δ_H (300 MHz, $CDCl_3$) 10.13 (2H, d, *J* 5), 8.79 (4H, m), 8.74 (2H, d, *J* 5), 5.62 (2H, s), 4.95 (2H, s), 4.26 (5H, s), −2.28 (2H, s). The second fraction (eluent hexane/DCM, 2:1) gave 5,10-bisferrocenyl-15,20-bis(pentafluorophenyl)porphyrin, **7** (36 mg, 4%), as a purple solid, mp >200 °C. Anal. Found: C, 61.74; H, 2.96; N, 5.58. $C_{52}H_{28}N_4F_{10}Fe_2$ requires C, 61.81; H, 2.79; N, 5.54. δ_H (300 MHz, $CDCl_3$) 10.05 (1H, d, *J* 5), 9.97 (2H, d, *J* 5), 9.83 (1H, m), 8.65 (4H, m), 5.53 (4H, m), 4.88 (4H, m), 4.16 (10H, m), −1.63 (1H, s), −1.73 (1H, s); λ_{max} (2.77×10^{-6} M in THF) 424 ($\epsilon = 2.20 \times 10^5$) nm.

[5,15-Bisferrocenyl-10,20-bis(pentafluorophenyl)porphyrinato]-zinc(II) (8) and [5,15-Bisferrocenyl-10,20-bis(pentafluorophenyl)-porphyrinato]nickel(II) (9). 5,15-Bisferrocenyl-10,20-bis(pentafluorophenyl)porphyrin (20 mg, 0.02 mmol) and zinc acetate dihydrate (3 equiv, 13 mg, 0.06 mmol) were added to *N*,*N*-dimethylformamide (10 mL), and the resulting solution was heated to reflux for 4 h. Then water (100 mL) was added to the mixture, and the precipitate was filtered. The resultant material was purified by column chromatography over silica (eluent hexane/DCM, 1:1) to give [5,15-bisferrocenyl-10,20-bis(pentafluorophenyl)porphyrinato] zinc(II) (**8**) (16 mg, 76%) as a dark brown solid, mp >200 °C. Anal. Found: C, 58.32; H, 2.63; N, 5.28. $C_{52}H_{26}N_4F_{10}Fe_2Zn$ requires C, 58.16; H, 2.44; N, 5.22. δ_H (300 MHz, $CDCl_3$) 10.21 (4H, d, *J* 5), 8.86 (4H, d, *J* 5), 5.53 (4H, t, *J* 2), 4.87 (4H, t, *J* 2), 4.24 (10H, s); λ_{max} (2.23×10^{-6} M in THF) 428 ($\epsilon = 2.33 \times 10^5$), 650 ($\epsilon = 1.16 \times 10^4$) nm.

[5,15-Bisferrocenyl-10,20-bis(pentafluorophenyl)porphyrinato]-nickel(II) (**9**) was synthesized in exactly the same manner utilizing nickel acetate dihydrate (3 equiv, 15 mg, 0.06 mmol) rather than zinc acetate, yielding 11 mg (62%) as a dark brown solid, mp >200 °C. Anal. Found: C, 58.29; H, 2.49; N, 5.31. $C_{52}H_{26}N_4F_{10}Fe_2Ni$ requires C, 58.52; H, 2.46; N, 5.25. δ_H (300 MHz, $CDCl_3$) 9.64 (4H, d, *J* 5), 8.52 (4H, d, *J* 5), 5.16 (4H, br s), 4.75 (4H, br s), 4.02 (10H, s); λ_{max} (7.49×10^{-7} M in THF) 421 ($\epsilon = 1.56 \times 10^5$) nm.

[5,10-Bisferrocenyl-15,20-bis(pentafluorophenyl)porphyrinato]-zinc(II) (10) and [5,10-Bisferrocenyl-15,20-bis(pentafluorophenyl)porphyrinato]nickel(II) (11). These *cis* derivatives were synthesized and isolated as described above for the corresponding *trans* derivatives by replacing **6** with **7** and using the chromatographic eluent hexane/DCM, 1:1.

Characterization data for dark purple **10**: Yield 93%. Anal. Found: C, 58.35; H, 2.68; N, 5.57. $C_{52}H_{26}N_4F_{10}Fe_2Zn$ requires C, 58.16; H, 2.44; N, 5.22%); δ_H (300 MHz, $CDCl_3$) 10.11 (3H, br m),10.01 (1H, s), 8.73 (4H, m), 5.64 (4H, br s), 4.95 (4H, br s), 4.24 (10H, m); λ_{max} (1.49×10^{-6} M in THF) 429 ($\epsilon = 2.61 \times 10^5$) nm.

Characterization data for dark purple **11**: Yield, 57%; (Found: C, 58.34; H, 2.51; N, 5.30. $C_{52}H_{26}N_4F_{10}Fe_2Ni$ requires C, 58.52; H, 2.46; N, 5.25. δ_H (300 MHz, $CDCl_3$) 9.57 (3H, br m), 9.47 (1H, s), 8.50 (4H, m), 5.58 (4H, br s), 4.85 (4H, br s), 4.11 (10H, s); λ_{max} (1.125×10^{-5} M in THF) 421 ($\epsilon = 2.49 \times 10^5$) nm.

Cyclic Voltammetry. CV experiments were performed on ca. 1 mM solutions of H_2tpp and **6**−**11** in dry CH_2Cl_2/0.100 M $[N(^nBu)_4][B(C_6F_5)_4]$, utilizing a standard three-electrode cell with glassy carbon electrode of surface area 7.07 mm^2 pretreated by polishing on a Buehler microcloth first with 1 μm and then 1/4 μm diamond paste, a Pt-wire counter electrode, and a Ag/Ag^+ reference electrode. The reference electrode was constructed by immersing a Ag wire in an acetonitrile solution containing 0.010 M $AgNO_3$ and 0.100 M $[N(^nBu)_4][B(C_6F_5)_4]$ in a thin inner Luggin capillary

(33) LeSuer, R. J.; Buttolph, C.; Geiger, W. E. *Anal. Chem.* **2004**, *76*, 6395.

with Vicor tip. This Luggin was immersed into a second Luggin capillary that contained a 0.100 M $[N(^nBu)_4][B(C_6F_5)_4]$ dichloromethane solution. All measurements were conducted under a blanket of argon at 25 °C in a Faraday cage connected to a BAS 100 B/W electrochemical workstation interfaced with a personal computer. Data, uncorrected for junction potentials, were collected with standard BAS 100 software and exported to Excel for manipulation and analyses. Successive experiments under the same experimental conditions showed that all formal reduction and oxidation potentials were reproducible within 5 mV. All potentials in this study were experimentally referenced against the Ag/Ag^+ couple but were then manipulated on Excel to be referenced against Fc/Fc^+ as recommended by IUPAC.[26] Under our conditions the Fc/Fc^+ couple exhibited $i_{pc}/i_{pa} = 0.94$, $\Delta E_p = 81$ mV, and $E^{\circ\prime} = 0.087$ V versus Ag/Ag^+. All temperatures were kept constant to within 0.2 °C.

Acknowledgment. The authors acknowledge the NRF under grant 2054243 and the UFS for financial support.

OM060373U